ACS APPLIED BIO MATERIALS
Cite This: ACS Appl. Bio Mater. 2019, 2, 3942−3953
Article
www.acsabm.org

Plasmonic Nanohybrid with High Photothermal Conversion Efficiency for Simultaneously Effective Antibacterial/Anticancer Photothermal Therapy

Muhammad Rizwan Younis,[†] Rui Bing An,[†] Yun-Chao Yin,[†] Shouju Wang,[‡] Deju Ye,[†] and Xing-Hua Xia*[,†]

[†]State Key Laboratory of Analytical Chemistry for Life Science, School of Chemistry and Chemical Engineering, Nanjing University, Nanjing 210023, China

[‡]Department of Radiology, The First Affiliated Hospital of Nanjing Medical University, Nanjing 210000, China

Supporting Information

ABSTRACT: Plasmonic metal/semiconductor nanohybrids hold great promise in photocatalysis and biosensor development; however, their potential phototherapeutic applications are yet fully unexplored. On the other hand, the demand of high laser power density to induce antibacterial photothermal therapeutic effects greatly restricts the practical applicability of the previously developed photothermal nanoagents (PTAs) for anticancer photothermal therapy (PTT). Here, we develop a plasmonic nanohybrid by integrating plasmonic noble metal gold nanorods (AuNRs) with a two-dimensional graphene oxide (2-D GO), capable to perform photothermal ablation of both bacterial pathogens as well as tumor cells, respectively, under low power single near-infrared (NIR) laser activation. Owing to the synergistic plasmonic photothermal effect (PPTT) of dual plasmonic PTAs, the plasmonic AuNR/GO nanohybrid exhibits remarkably higher photothermal conversion efficiency (PCE, 72.59%) than either individual AuNRs or GO under low laser power density (300 mW), leading to enhanced antibacterial/anticancer PTT. In addition, the synergistic plasmonic antibacterial/anticancer PTT induced by the plasmonic nanohybrid is also far superior to individual PTAs (AuNRs or GO), whereas the flow cytometric analysis of heat shock proteins (HSP 70) clearly dictates that the substantial killing of bacterial pathogens/tumor cells is solely due to the synergistic PPTT. Thus, the plasmonic AuNR/GO nanohybrid is a standalone PTA to perform simultaneous antibacterial/anticancer PTT under low power NIR laser activation for only 5 min, without any systemic side effects. The present study provides a clear demonstration about the potential therapeutic impact of plasmonic nanohybrids and thus will surely pave the way to design other hybrid nanoagents with enhanced PCE and integrate them with chemotherapeutic agents, leading to dual-modal chemo-/photothermal antibacterial/anticancer therapy under low power single laser excitation for a short duration.

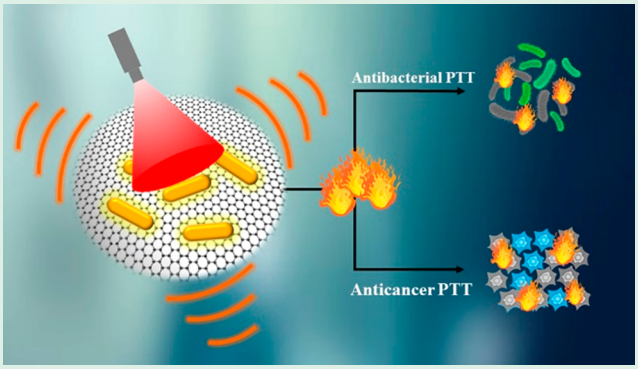

KEYWORDS: *plasmonic nanohybrid, photothermal conversion efficiency, plasmonic photothermal therapy, laser power density, heat shock proteins*

INTRODUCTION

Being a leading cause of mortality, cancer and notorious bacterial pathogen induced severe infections have become a potential threat to the lives of human beings on this planet.[1−3] To fight the spread of such life-threatening diseases, chemotherapy is the most widely accepted approach to cure a diverse range of malignancies and remove the bacterial pathogens.[4−6] However, systemic cytotoxic side effects associated with the chemotherapeutic drugs and the emergence of multidrug-resistant bacteria due to an excessive usage of antibiotics raise a big question about the safety as well as the practical utility and efficacy of this approach.[7,8] Thus, significant efforts have been made to develop an alternative approach such as synthesizing new antibiotics and light-activated therapy, especially photodynamic/photothermal therapy of bacterial pathogens/cancer.[9,10] As the strict dependence of PDT on molecular oxygen greatly limits its practical applicability,[11,12] photothermal therapy (PTT) has emerged as a promising strategy to effectively treat bacterial infections and cancer.[13−15] In PTT, a photothermal nanoagent (PTA) directly converts the absorbed laser energy into heat and thus generates localized hyperthermia, enabling photothermal killing of bacterial pathogens/tumor cells. As PTA is solely responsible for high PTT efficacy, a number of PTAs have been recently developed for the PTT

Received: June 14, 2019
Accepted: August 19, 2019
Published: August 20, 2019

DOI: 10.1021/acsabm.9b00521
ACS Appl. Bio Mater. 2019, 2, 3942−3953

of tumor malignancies and bacterial infections, respectively.[16−18] However, a single photothermal nanoagent capable of performing simultaneous photothermal killing of bacterial pathogens/cancer cells is surprisingly rare. The main hurdle is the laser power density, as high laser power could possibly be employed for bacterial PTT, but it is strongly discouraged in the case of cancer PTT owing to the risk of potential skin burns and damages to the normal tissues. Therefore, a PTA agent which could be applied for antibacterial PTT is not suitable for anticancer PTT. There is a great demand of single dual modal PTAs, which can simultaneously perform antibacterial/anticancer PTT under low power laser activation, enabling a simple, more translational, and practically feasible therapeutic approach.

Owing to the fascinating physicochemical characteristics and superior functionalities compared to their individual counterparts, plasmonic metal/semiconductor nanohybrids demonstrate promising applications in water splitting,[19] photoelectrochemical biosensing,[20] photovoltaics,[21] photocatalysis,[22] and nanomedicine.[23−25] To take advantage of the striking features of the plasmonic noble metals such as strong light−matter interactions and localized surface plasmon resonance phenomena, they are usually integrated with a semiconductor material, and thus the resultant plasmonic nanohybrid demonstrates low charge carrier recombination and enhanced light absorption capacity, leading to an efficient transformation of the laser energy into either electrical, magnetic, or thermal energy, respectively.[26] Among the plasmonic noble metals (e.g., Au, Ag, Cu), different gold (Au) nanostructures, particularly gold nanorods (AuNRs), hold great promise in drug delivery and antibacterial/anticancer PTT because of their ease in synthesis, biocompatibility, high extinction coefficients, tunable longitudinal localized surface plasmon resonance (LSPR) band at the NIR region, high PCE, and excellent photothermal stability.[27,28] Previously, plasmonic nanohybrids consisting of different Au nanostructures have been designed for either antibacterial or anticancer PTT, respectively, but complicated synthesis protocols and the demand of high power NIR laser excitation to generate extensive localized hyperthermia seriously restrict their anticancer PTT applications *in vivo*.[29,30] To address this problem, we recently provided an effective design consisting of a plasmonic Au/MoS_2 hybrid to perform synergistic antitumor PDT/PTT under single low-power NIR laser activation for 5 min.[31] Due to the synergistic PPTT effects induced by AuNR/MoS_2, a high PCE (68.8%) was achieved, leading to remarkable antitumor PTT efficacy *in vivo*. Earlier, we also demonstrated the tremendous applications of LSPR phenomena to enhance hydrogen evolution reaction (HER) performance as well as improved photoelectrochemical (PEC) biosensing activity of the plasmonic nanohybrid.[20,32] Thus, our previous findings and the understanding of the LSPR phenomenon encourage us to further extend our investigations and explore the potential of plasmonic nanohybrids for simultaneous antibacterial/anticancer PTT.

Apart from Au-based plasmonic materials, graphene oxide (GO) is a sheet-like 2-D material and has gained increasing attention owing to an excellent thermal and electrical conductivity, outstanding physicochemical characteristics, facile surface functionalization, and strong mechanical strength and thus makes a substantial impact on the electronic industry (optoelectronics, supercapacitors, and solar cells) and sensor development.[33,34] Additionally, owing to the high surface area, water dispersibility, biocompatibility, and photothermal properties, GO and GO/nanoparticle hybrids showed promising potential in biosensing and cancer theranostics (imaging, drug delivery, and PTT).[35] However, integration of plasmonic materials with GO is a promising approach to achieve high PTT efficacy.[36] For instance, Liu and co-workers integrated copper sulfide (CuS) with GO to enhance PTT efficiency. Due to the high surface area of GO, ICG dye was loaded onto the GO/CuS hybrid, resulting in high therapeutic performance due to the synergistic PDT/PTT.[37] Apart from the PDT agent, Jiang et al. loaded a chemotherapeutic drug (doxorubicin, DOX) onto the PEG-GO/CuS nanocomposite, demonstrating excellent therapeutic outcomes against a cervical tumor due to the synergistic chemo/PTT.[38] Recently, Liu's group developed a single laser-activated phototherapeutic nanoplatform by integrating gold nanostars with GO instead of CuS (GO/AuNSs) and loaded with PDT agent (Ce6). Notably, under single 660 nm laser activation, the designed nanoplatform demonstrated dual-modal imaging (photothermal/fluorescence) guided synergistic PDT/PTT against the EMT6 tumor, resulting in complete eradication of the EMT6 tumor *in vivo*.[39] Though an improved therapeutic performance has been shown by the GO/AuNSs-PEG/Ce6, the lower tissue penetration depth of 660 nm laser light is a major hindrance in practical clinical applications.

As light penetration depth within the tissue is significantly higher in the NIR region, we chose AuNRs due to their facile tunable absorption in the NIR region. Thus, herein, a plasmonic nanohybrid by integrating plasmonic noble metal gold nanorods (AuNRs) with a 2-D GO has been developed for simultaneous antibacterial/anticancer PTT under low-power, near-infrared (NIR) laser activation. Plasmonic AuNRs were electrostatically assembled onto GO nanosheets via the facile sonication approach, forming the plasmonic AuNRs]/GO nanohybrid. By considering the practical applicability of the designed nanohybrid for anticancer PTT, the longitudinal LSPR band of AuNRs was successfully tailored into the NIR region, enabling deeper tissue penetration depth. Notably, owing to the synergistic PPTT effects, the AuNR/GO nanohybrid exhibits higher PCE than either individual AuNRs or GO, leading to substantial PTT killing of both HeLa tumor cells as well as Gram +ve and Gram −ve bacteria under low power NIR laser activation for a short time period. In addition, an enhanced expression of the heat shock proteins (HSP 70) clearly reveals that plasmonic PTT is solely responsible for the destruction of bacterial pathogens/tumor cells. The current study demonstrates an effective approach to achieve antibacterial/anticancer PTT using single plasmonic nanohybrid-based PTAs under low power laser excitation.

EXPERIMENTAL SECTION

Materials. All the chemicals were of analytical grade and used as per supplier instructions without any further purification. Pure graphite powder (99.9%) was purchased from Alfa Aesar. Sulfuric acid (H_2SO_4), polyethylene glycol (PEG-400), sodium oleate (NaOL), hydrogen peroxide (H_2O_2), sodium borohydride ($NaBH_4$), and ethanol were bought from Sinopharm Chemical Reagent Co., Ltd. Phosphorus pentoxide (P_2O_5), potassium persulfate ($K_2S_2O_8$), and potassium permanganate ($KMnO_4$) were obtained from Nanjing Chemical Reagent Co., Ltd. (Nanjing, China). Hydrochloric acid (HCl) was obtained from Shanghai Lingfeng Chemical Reagent Co., Ltd. Tetrahydrate gold chloride ($HAuCl_4 \cdot 4H_2O$) was provided by the First Reagent Factory (Shanghai, China). Ascorbic acid (AA), hexadecyl trimethylammonium bromide

DOI: 10.1021/acsabm.9b00521
ACS Appl. Bio Mater. 2019, 2, 3942−3953

(CTAB), and silver nitrate ($AgNO_3$) were bought from Sigma-Aldrich and Johnson Matthey Corporation, respectively. Methyl thiazolyl-tetrazolium (MTT), phosphate buffer saline (PBS, pH 7.4), and dimethyl sulfoxide (DMSO) were procured from Keygen Biotech. Co., Ltd. Fetal bovine serum (FBS) and HeLa cell culture medium such as Dulbecco Modified Eagle's Medium (DMEM) were provided by Hyclone. For solution preparations, deionized water (DI H_2O, 18.2 MΩ·cm) was used throughout the study.

Synthesis of PEGylated 2-D GO Nanosheets. First, GO was prepared by following the reported protocol by Wang et al.[40] In detail, 6 g of graphite powder, 3 g of $K_2S_2O_8$, and 3 g of P_2O_5 were mixed in a concentrated H_2SO_4 and heated at 80 °C for about 8 h. Next, 3 g of $KMnO_4$ and 23 mL of concentrated H_2SO_4 were added slowly to oxidize the resultant graphite. Notably, the reaction was performed in an ice bath to keep the reaction temperature below 10 °C. Later, the suspension was transferred to a water bath set at 35 °C and stirred for about 2 h. Afterward, 40 mL DI of H_2O was added slowly by dropping a funnel, and the solution was refluxed and heated at 95 °C for at least 30 min. Then, 100 mL of DI H_2O and 30% H_2O_2 (0.003 L) were added slowly to terminate the reaction, and the resulting suspension turned from dark brown to yellow. Finally, the yellow suspension was filtered with a 0.22 μm membrane and washed three time with 200 mL each of HCl (1 M) and DI H_2O, respectively. The as-synthesized GO was vacuum-dried at 50 °C for 1 day prior to storage for further use. For PEGylation, aqueous solution of PEG-400 (25 mg) with pH = 9 was mixed at room temperature (RT) with 1 mg/mL of aqueous dispersion of GO and stirred for almost 12 h. Thereafter, PEGylated GO was retrieved via centrifugation (8000 rpm, 3 times) with DI H_2O. The resultant pellet was freeze-dried overnight prior to storage at RT for further use.

Synthesis of AuNRs with the LSPR Band at 756 nm. AuNRs with a localized surface plasmon resonance (LSPR) band at 756 nm were prepared by following the well-established seed-mediated approach reported elsewhere.[41] Briefly, 0.1 M CTAB (5 mL) and 1% of $HAuCl_4$(100 μL) were mixed prior to the addition of freshly prepared ice-cold 0.01 M $NaBH_4$ (0.6 mL) under vigorous stirring. After an immediate color change as mentioned previously,[31] which indicates the formation of Au seeds, the resultant seed solution was kept for almost 2 h at RT to ensure the hydrolysis of unreacted $NaBH_4$. Next, AuNRs were prepared by the sequential addition of different reagents into the 250 mL flask in the following order: 0.1 L of CTAB (0.1 M), 1 mL of $AgNO_3$ (0.1 M), 1% $HAuCl_4$ (200 mL), and 200 μL of 1 M HCl. All the above-mentioned reagents were mixed gently by stirring at RT, followed by adding 0.8 mL of AA (0.0788 M) as a reducing agent. Finally, 120 μL of the previously prepared Au seed solution was added, and the solution was kept at 30 °C in a water bath overnight. The resultant AuNRs were purified three times via centrifugation (8000 rpm) for 15 min, and the pellet was collected and stored for further use.

Fabrication of the AuNR@GO Nanohybrid. For the synthesis of the AuNR@GO nanohybrid, an aqueous suspension of both PEG-GO and AuNRs was added in a falcon tube at a volume ratio of 2:1. The resultant mixture was undergoing sonication for at least 2 h at RT and then was purified via centrifugation with DI H_2O. Finally, the pellet was freeze-dried for about 14 h.

Characterization. Light absorption measurements were performed using a UV-1800 spectrophotometer (Shimadzu). Morphological characterization, elemental mapping, and energy-dispersive X-ray (EDX) analysis of AuNRs, GO, and AuNR/GO were performed on a scanning electron microscopy (SEM, JEOL-2100, Japan) by drying a very dilute concentration of each sample on silicon wafer. Surface zeta potential and DLS analysis were acquired by using Malvern Zetasizer Nano ZS90 at RT. Raman and X-ray photoelectron (XPS) spectroscopic characterizations were acquired using FT-Raman Spectrometer (Bruker) and PHI 5000 VersaProbe (Japan), respectively. The thickness of GO sheets was determined by using atomic force microscopy (AFM, Bruker), and Fourier transform infrared spectroscopy (FTIR, Thermo Fisher Scientific, Inc.) was employed to characterize the functional groups of GO.

Photothermal Profiling. To assess the photothermal (PTT) performance *in vitro*, aqueous dispersions (100 μg/mL) of each AuNR, GO, and the AuNR/GO nanohybrid underwent CW NIR laser excitation (808 nm, 300 mW) for 5 min. The real time−temperature increase in the aqueous solution of each sample was measured by an infrared (IR) thermal imaging camera, and the temperature data were analyzed as mentioned previously.[31] Meanwhile, the PTT performance of the AuNR/GO hybrid under different concentrations (10, 20, 50, and 100 μg/mL) and the photothermal stability of the AuNR/GO nanohybrid were also investigated under four sequential laser on/off cycles. Similarly, laser power (100, 300, 500, and 750 mW) dependent PTT performance of the AuNR/GO nanohybrid was also determined under similar conditions as mentioned above. However, PBS was used as a control.

Calculation of Photothermal Performance. To determine the photothermal conversion efficiency (PCE), 100 μg/mL of each AuNR, GO, and the AuNR/GO nanohybrid, respectively, was irradiated by a NIR laser (300 mW) until the temperature reached a steady state. Then, the laser system was switched off, allowing the solution to cool down. Thereafter, PCE (η) was calculated using the following formula

$$\eta = \frac{hS(T_{max} - T_{surr}) - Q_o}{I(1 - 10^{-A})} \quad (1)$$

where h is the coefficient of heat transfer; S is the surface area; T_{max} is the maximum temperature; and T_{surr} refers to the surrounding temperature, respectively. Heat absorbed by the tube and the laser power density are denoted by Q_O (83 mW) and I (0.3 W/cm^2), respectively, while the optical density of each material is represented by A (OD = 0.5).

When the heat input is equal to the heat output, we determined the hS using the following equation

$$hS = \frac{\sum_i m_i C_{p,i}}{\tau_s} \approx \frac{m_{H_2O} C_{H_2O}}{\tau_s} \quad (2)$$

where m_{H2O} is the weight and C_{H2O} is the specific heat capacity of water. The heat dissipation time constant is denoted by τ_s.

The linear data of the cooling period were plotted with the negative natural logarithm to determine τ_s using the following equation:

$$t = -\tau_s \ln \theta = \tau_s \ln \frac{T - T_{surr}}{T_{max} - T_{surr}} \quad (3)$$

Cellular Experiments. For cellular studies, HeLa tumor cells and the normal human cell line (HUVECs)[31] were obtained from Procell Life Science and Technology Co., Ltd. (Wuhan, China). Both the cells were cultured following supplier instructions and kept in a 5% CO_2 humidifier incubator at 37 °C.

Cellular Uptake Study. *In vitro* cellular uptake of the AuNR/GO nanohybrid was examined using an inverted fluorescence microscope (Olympus IX73, Japan). However, FITC dye was functionalized with a plasmonic nanohybrid, and thus, the fluorescence of FITC was tracked to monitor the uptake of AuNRs/GO *in vitro*. Briefly, specific concentrations of FITC were mixed at RT with 1 mg/mL of AuNRs/GO under stirring for almost 2 h. Afterward, the AuNR/GO nanohybrid was centrifuged at 8000 rpm for 0.25 h, and the supernatant containing unbound FITC was discarded. The pellet containing FITC-functionalized AuNRs/GO was stored for further *in vitro* studies. For the investigation of *in vitro* cellular uptake, HeLa cells at a density of 1×10^5 were seeded in a 35 mm culture dish and supplemented DMEM culture media with 10% FBS (1 mL) for 24 h. Afterward, the fresh culture medium containing 100 μg/mL of the FITC-bounded AuNR/GO nanohybrid was added and incubated for specific time intervals (0.5, 2, 6, 12, and 24 h). After incubation, cellular uptake was analyzed by *in vitro* fluorescence imaging using an inverted fluorescence microscope. Similarly, concentration-dependent cellular uptake of the AuNR/GO nanohybrid (10, 20, 50, and 100 μg/mL) was also determined under similar conditions.

DOI: 10.1021/acsabm.9b00521
ACS Appl. Bio Mater. 2019, 2, 3942−3953

Scheme 1. Graphical Representation of the Fabrication Protocol of the Plasmonic AuNR/GO Nanohybrid and the Demonstration of Simultaneous Antibacterial/Anticancer PTT by AuNRs/GO under Laser Excitation (808 nm, 300 mW)

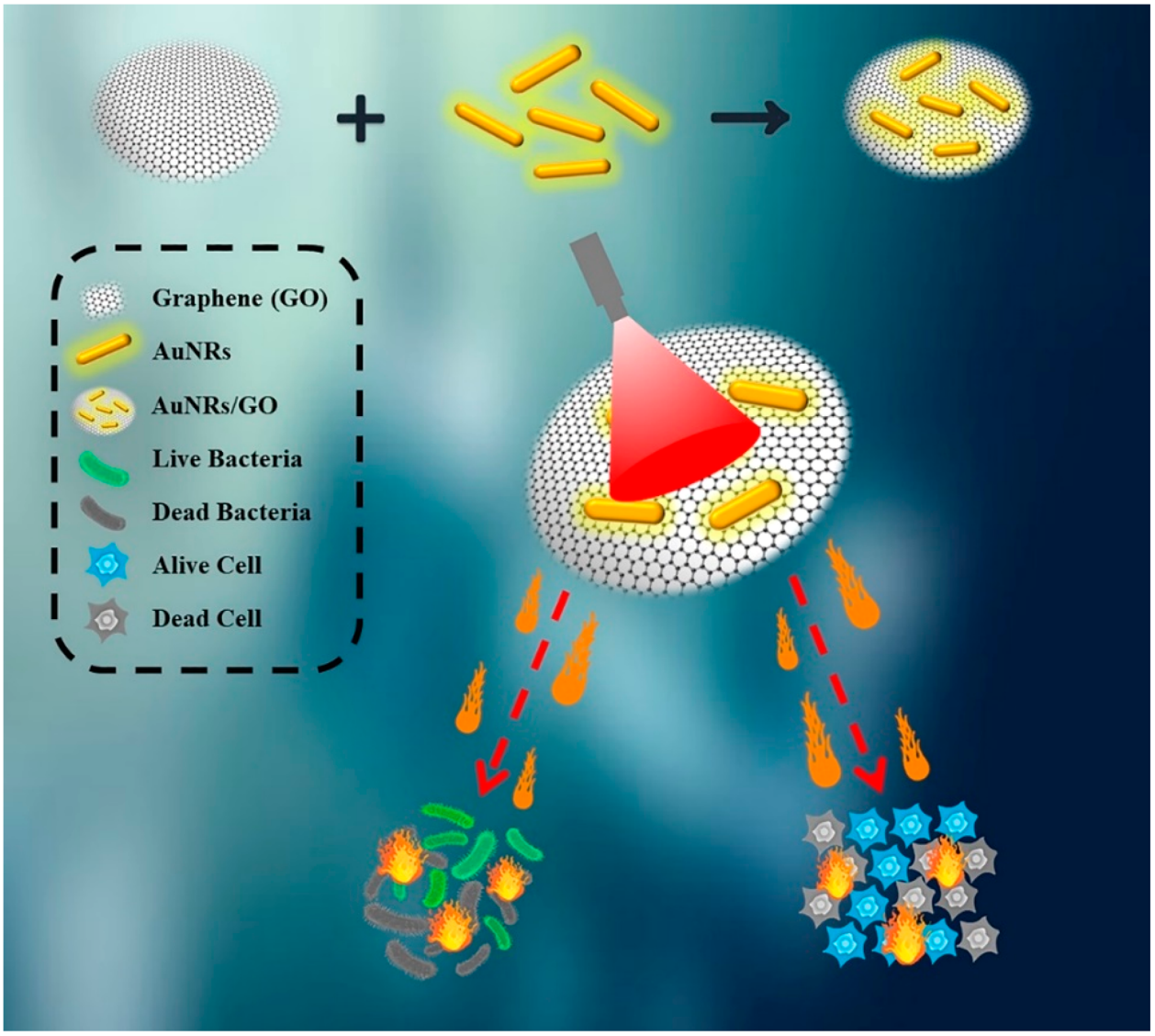

In Vitro Stability. Phosphate buffer saline with 10% FBS media was used to examine the stability of the hybrid material. Particularly, AuNR/GO was added into the above-mentioned media, and the UV−vis absorption was recorded at different time points (0, 2, 6, 12, 24, 48, and 72 h) using UV−vis absorption spectroscopy.

In Vitro Biocompatibility and Anticancer PTT. First, the biocompatibility of different concentrations of the AuNR/GO (10, 20, 50, and 100 μg/mL) nanohybrid was investigated *in vitro* under dark conditions against HUVECs and HeLa tumor cells.[31] Next, concentration-dependent *in vitro* anticancer PTT performance was determined under light irradiation by MTT assay following the supplier instructions. Briefly, 5×10^3 HeLa cells/well were seeded in 96-well plates and incubated overnight at 37 °C. Then, the fresh culture medium was added, containing the above-mentioned different concentrations of the AuNR, GO, and the AuNR/GO nanohybrid, and incubated for 4 h. Next, each well underwent NIR laser irradiation for 300 s and was incubated for another 24 h. Thereafter, an MTT agent was added following the reported literature,[31] and the quantitative determination of the cellular viability was made by monitoring the absorbance in each well using a microplate reader at 550 nm. In addition, therapeutic performance was also investigated by the Live/Dead assay under similar conditions using Calcein AM/PI costaining as per supplier instructions.

Expression Analysis of Heat Shock Proteins (HSP-70). For the flow cytometric expression analysis of the HSP-70, 1×10^5 HeLa cells were seeded in a 6-well plate, supplemented with culture medium (DMEM), and incubated for 24 h at 37 °C. Next, fresh DMEM medium was added containing different concentrations of the AuNR/GO nanohybrid and incubated for a further 8 h. Thereafter, all the wells were subjected to the 808 nm laser irradiation (300 mW) for 5 min. Then, the cells underwent a trypsinization procedure, were washed with PBS and stained with HSP-70 conjugated dye (Alexa fluor), and incubated for half an hour. At last, all the wells were rinsed, washed, and resuspended in PBS for flow cytometric analysis. As a control, the expression of HSP-70 of HeLa cells was kept under dark conditions and was also monitored under similar conditions.

In Vitro Antibacterial PTT. Antibacterial activity of the plasmonic AuNRs/GO nanohybrid was assessed against *Staphylococcus aureus* (*S. aureus*, Gram-positive) and *Escherichia coli* (*E. coli*, Gram-negative) bacteria. Both ATCC 25923 (*S. aureus* stain) and ATCC 25922 (*E. coli* stain), respectively, were obtained from Shenzhen University, Shenzhen, Guangdong, China. Typically, Luria−Bertani broth (LB) medium for bacterial culture was prepared by peptone (1%), beef extract (0.5%), and NaCl (0.5%), and the pH was adjusted to 7.2. All the glassware underwent a thorough sterilization procedure prior to bacterial culture. Then, *S. aureus* and *E. coli* were inoculated into the

DOI: 10.1021/acsabm.9b00521
ACS Appl. Bio Mater. 2019, 2, 3942−3953

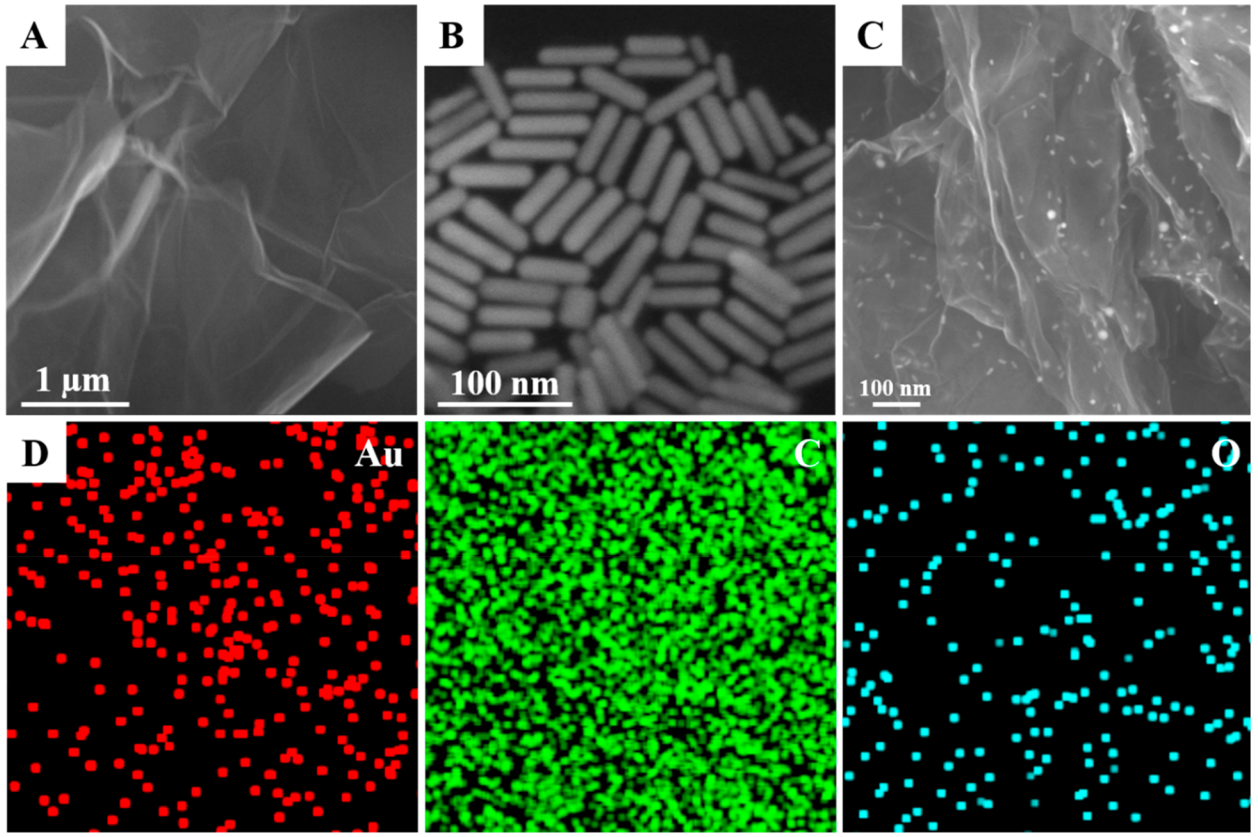

Figure 1. Characterization of plasmonic the AuNR/GO nanohybrid. SEM images of AuNRs (A), GO nanosheets (B), and the plasmonic AuNR/GO nanohybrid (C). SEM mapping of the plasmonic AuNR/GO nanohybrid (D).

fresh culture tubes with 5 mL of LB broth medium and grown in an aerobic condition overnight at 37 °C under continuous shaking. The growth of bacterial cultures was optimized to obtain 0.4 OD at a wavelength of 600 nm. However, the bacterial concentrations of ~10^7–10^8 CFU/mL were achieved via sequential centrifugation at 6000 rpm (3 times) and washing with 10 mL of 5% NaCl. Next, the bacterial suspensions of *S. aureus* and *E. coli*, respectively, were mixed with 100 μg/mL of AuNRs, GO, and AuNR/GO and vortexed for at least 10 min to ensure efficient interaction of nanomaterials with bacterial samples. Then, all the samples underwent washing via centrifugation (10 000 rpm, 10 min), and the pellets containing bacterial samples with nanomaterials were stored for further *in vitro* antibacterial PTT studies.

To determine the antibacterial PTT efficacy, both the bacterial samples were treated with 808 nm laser irradiation (300 mW) for 5 min. Afterward, a serial dilution of all the samples was performed, and they were mixed with NaCl solution (1%) to make a total volume of 1 mL. An aliquot was withdrawn from each sample solution, streaked on LB broth medium, and incubated overnight under dark conditions at 37 °C to assess the bacterial viability via the colony forming unit (CFU). Bacterial samples in the dark or only under light irradiation were used as a control, respectively.

In Vivo Bbiocompatibility. To assess the cytotoxicity and potential side effects, *in vivo* biocompatibility investigations were carried out on healthy nude mice, divided randomly into either saline (group 1) or an experimental group (group 2), respectively. Group 1 received 100 μL of saline, while group 2 received an i.v. injection of 100 μg/mL of AuNR/GO (100 μL). The body weight of all the mice in either group 1 or 2 was monitored every 2 days and after 18 days, and blood and major body organs, e.g., spleen, intestine, kidney, liver, stomach, and heart, were collected by sacrificing all the mice. Then, blood biochemistry analysis as well as histopathological examination of the major organs were made by hematoxylin and eosin (H&E) staining, respectively, following the reported literature.[31]

Statistical Analysis. Unless otherwise stated, the data were presented as the mean and the standard deviation (SD) of three independent experiments. For statistical comparisons, GraphPad Prism 6 software was employed to perform Student's *t* test.

RESULTS AND DISCUSSION

The plasmonic AuNR/GO nanohybrid synthesized by facile electrostatic interactions to perform simultaneous antibacterial/anticancer PTT is illustrated in Scheme 1. Briefly, few-layered thick GO nanosheets (NSs) were first prepared by following the modified Hummer's method, as characterized by SEM (Figure 1A). The SEM mapping as well as EDX spectroscopic analysis confirm the presence of C and O elements, respectively (Figures S1A and S2A). Zeta potential analysis indicates that the GO nanosheets possess a negative surface zeta potential value (−39.62 mV) (Figure S3B), which is possibly due to the presence of carboxyl groups (COOH) as indicated by FTIR spectroscopic measurements. The characteristic absorption peaks of carbonyl groups (C═O) and C═C appear at 1616 and 1718 cm^{-1}, respectively, which correspond to the stretching vibration of −COOH groups at the edges of GO and the sp^2 network present in the basal plane of GO. In addition, an epoxy peak (C−O) at 1038 cm^{-1} as well as a broad peak at 3152 cm^{-1} (O−H stretching) are also observed as shown in Figure S4. Though the as-prepared GO nanosheets show excellent water dispersibility (Figure S5), PEG was functionalized with GO nanosheets to ensure their biocompatibility and suitability for biological applications.

By following the well-developed seed-mediated approach, AuNRs having an average length of 40 nm and a width of 13 nm, respectively, were prepared with an aspect ratio of 3.07 as

DOI: 10.1021/acsabm.9b00521
ACS Appl. Bio Mater. 2019, 2, 3942−3953

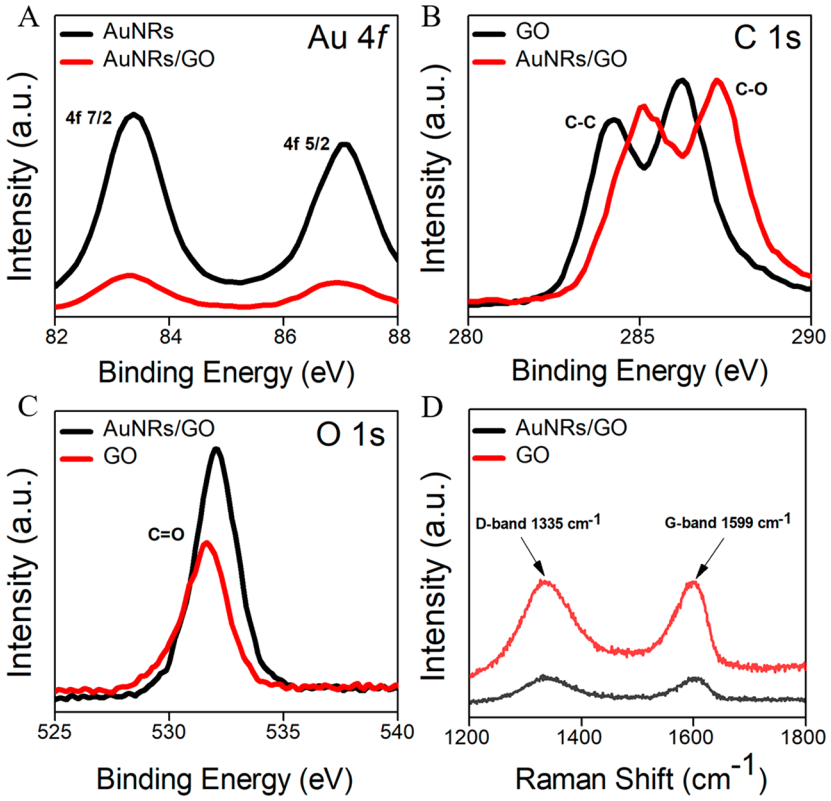

Figure 2. XPS and Raman characterizations of the plasmonic AuNR/GO nanohybrid. (A) XPS spectra of AuNRs and the AuNR/GO nanohybrid in the Au 4f region. (B,C) XPS spectra of GO and the AuNR/GO nanohybrid in the C 1s and O 1s regions. (D) Raman spectra of GO nanosheets and the AuNR/GO nanohybrid.

determined by SEM and DLS (Figure 1B and Figure S3A). Both the SEM mapping and EDX spectroscopic analysis confirm the presence of the Au element (Figure S1B and S2B). Owing to the CTAB surface stabilization, AuNRs exhibit a positive (+27.8 mV) surface zeta potential (Figure S3B). Thus, AuNRs have been decorated on the GO nanosheets (GO NSs) via electrostatic interactions, as the SEM image reveals the random decoration of AuNRs onto GO NSs (Figure 1C) with a low amount of AuNRs (3.2 and 2.97 wt %) that avoids the plasmonic coupling and aggregation as determined by EDX and ICP (Figure S2C).

The SEM elemental mapping further indicates the presence of Au, C, and O elements (Figure 1D), confirming the preparation of a plasmonic nanohybrid. Thus, the resultant AuNRs@GO exhibits an average hydrodynamic diameter of 173 nm with an overall positive surface zeta potential (10.37 mV), respectively, as determined by DLS and zeta potential analysis (Figure S3A,B). XPS and Raman spectroscopy were further employed to confirm the synthesis of the plasmonic AuNR/GO nanohybrid. Figure 2A shows the XPS spectrum of Au 4f measured from the AuNRs and AuNRs/GO, respectively. In the case of AuNRs, two spin−orbit doublets such as Au $4f^{7/2}$ and $4f^{5/2}$ are seen at 83.37 and 87.125 eV, respectively. However, a negative shift of 0.12 and 0.25 eV is noticed in the binding energy of these doublets, respectively, indicating a strong interaction between AuNRs and GO NSs. In contrast, the C 1s as well as O 1s spectra of AuNRs/GO reveal a positive shift in the peaks of sp^3 (C−C, 0.85 eV), epoxy (C−O, 1 eV), and carbonyl (C═O, 0.40 eV) functional groups as compared to GO NSs, respectively (Figure 2B,C). It is notable to mention that the peak intensities of the different functional groups presented in C 1s and O 1s did not decrease after AuNR binding, suggesting that the loading of AuNRs neither disturbs nor damages the structure of the GO NSs. The Raman spectra of the GO NSs show two characteristic Raman peaks at 1337 and 1602 cm^{-1}, attributed to the D and G bands, respectively. Particularly, the D and G bands correspond to the defects induced in the A_{1g} in-plane zone-edge mode and E_{2g} mode, respectively. However, binding of AuNRs onto GO NSs changes the in-phase vibration of both the bands as well as the induced phonon stiffening effect, resulting in red-shifted D (2 nm, 1337 cm^{-1}) and G bands (3 nm, 1602 cm^{-1}), respectively (Figure 2D).

UV/vis-NIR characterization study shows that GO NSs do not possess any characteristic absorption peak in the entire UV/vis-NIR region, while AuNRs exhibit characteristic transverse and longitudinal LSPR absorption bands at 514 and 760 nm, respectively. Upon loading of AuNRs onto GO nanosheets, the resultant AuNR/GO hybrid demonstrates an obvious red-shift (774 nm) in the LSPR band, which suggests that the dielectric environment of AuNRs has been changed owing to the presence of electrostatically assembled GO nanosheets (Figure 3A). The optical characterizations clearly demonstrate the successful synthesis of the plasmonic AuNR/GO nanohybrid via electrostatic interactions, capable of promoting a synergistic plasmonic photothermal effect. After the successful formation of the plasmonic AuNR@GO nanohybrid, the photothermal performance of individual AuNRs, GO nanosheets, and the AuNR@GO nanohybrid was evaluated. Compared to individual GO nanosheets (35.5 °C) and AuNRs (40.6 °C), the plasmonic AuNR@GO nanohybrid demonstrates a significant temperature increase

DOI: 10.1021/acsabm.9b00521
ACS Appl. Bio Mater. 2019, 2, 3942−3953

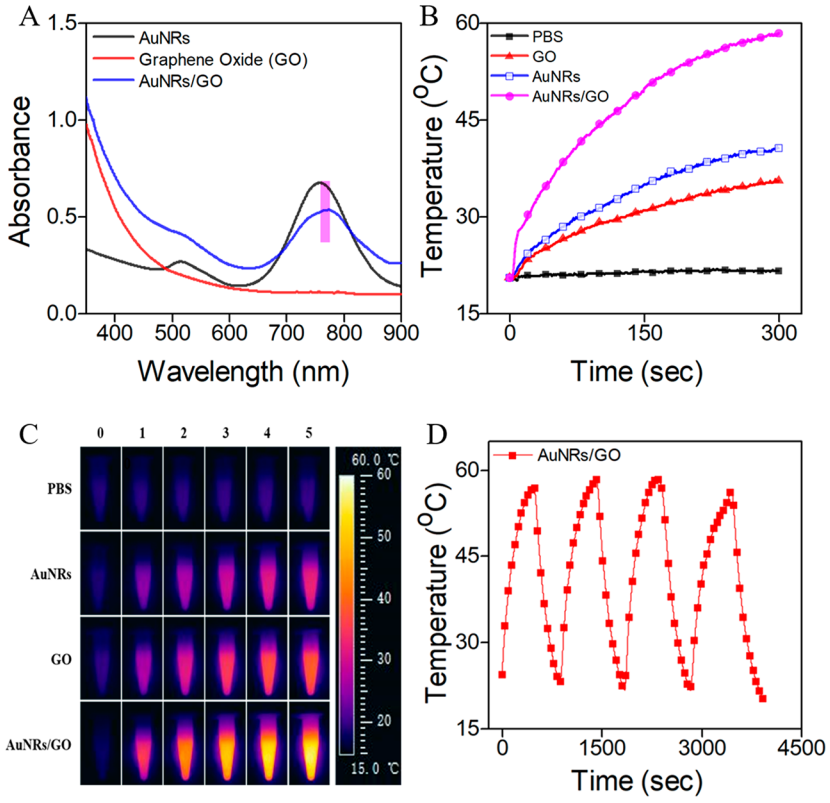

Figure 3. UV/vis characterization and *in vitro* PTT profiling. (A) UV/vis absorption profile of AuNRs, GO NSs, and the AuNR/GO hybrid. (B) *In vitro* PTT profiling of 100 μg/mL of GO nanosheets, AuNRs, and the AuNR/GO nanohybrid under 808 nm laser excitation (300 mW). (C) Digital photographs of the real-time temperature increase by the indicated groups as mentioned. (D) Photothermal stability of the AuNR/GO nanohybrid for four successive laser on/off cycles under similar conditions. PBS was used as a control.

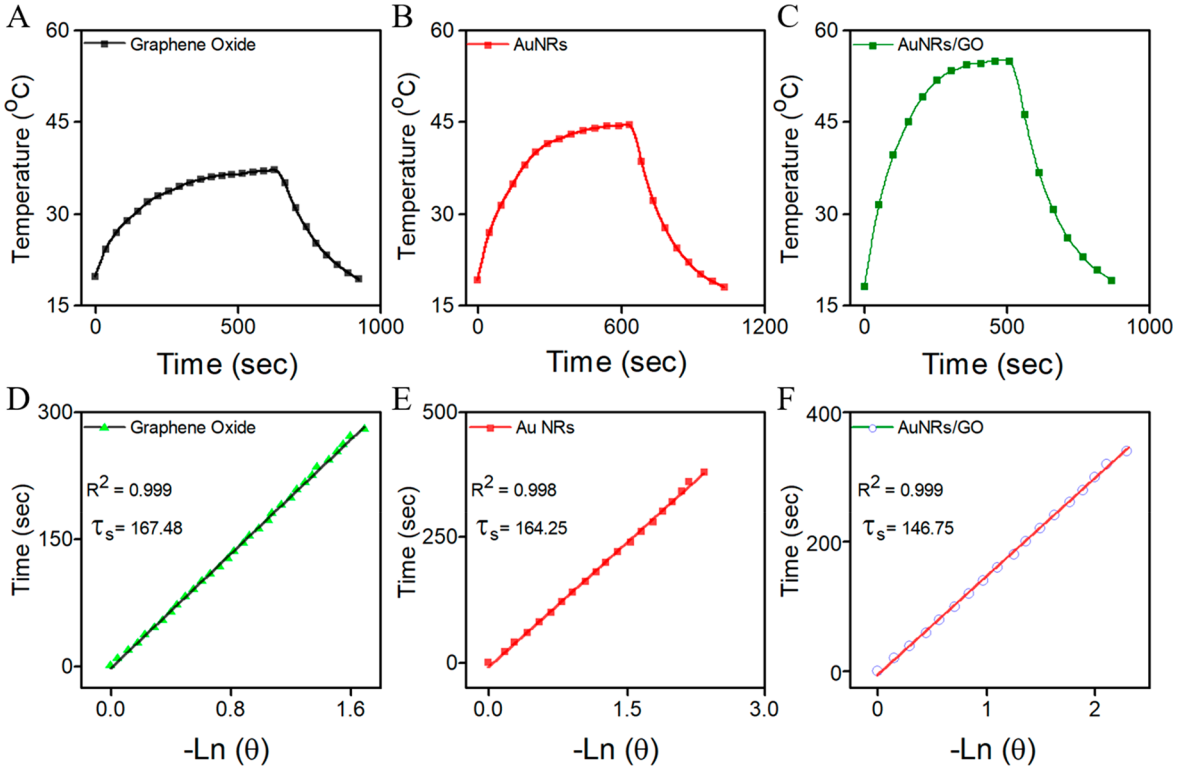

Figure 4. Photothermal conversion efficiency. (A–C) PCE calculations of the GO, AuNRs, and AuNR/GO nanohybrid. Heat dissipation time constants for each sample were calculated by plotting the negative natural log of the cooling period with time (D–F). All the materials received 808 nm laser irradiation (300 mW) for 5 min.

DOI: 10.1021/acsabm.9b00521
ACS Appl. Bio Mater. 2019, 2, 3942–3953

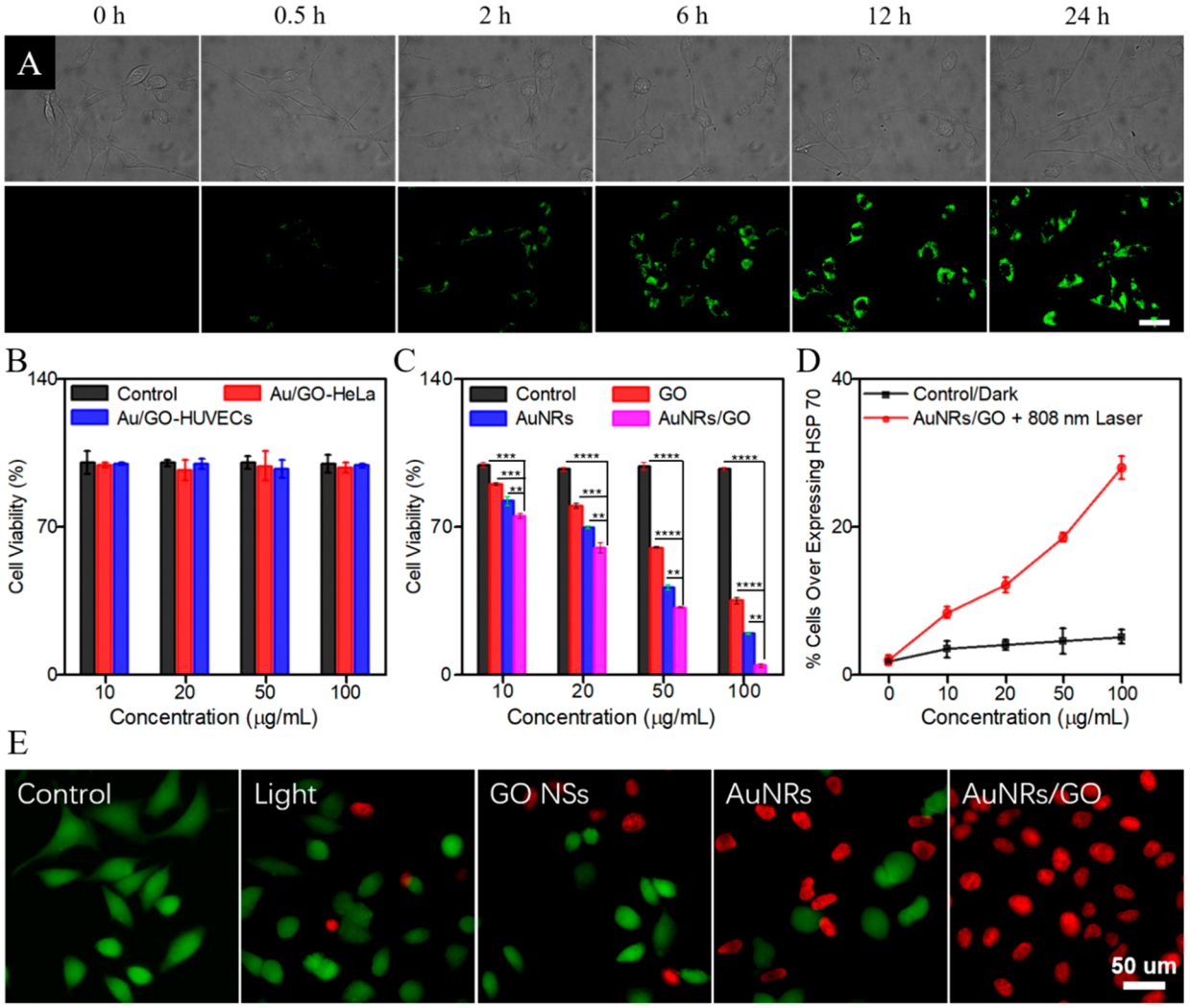

Figure 5. *In vitro* cellular uptake and antitumor PTT. (A) Time-dependent (0, 0.5, 2, 6, 12, and 24 h) increase in the fluorescence intensity of FITC in HeLa cells treated with 100 μg/mL of the AuNR/GO nanohybrid. Excitation/emission wavelength of FITC was Ex/Em = 495/519 nm. Scale bar is 50 μm. (B) Concentration-dependent dark cytotoxicity of the AuNR/GO nanohybrid against HUVECs and HeLa cells as mentioned. (C) Phototherapeutic killing performance of the indicated materials under 808 nm laser excitation (300 mW) for 5 min (**P < 0.01, ***P < 0.001, ****P < 0.0001). (D) Overexpression of heat shock proteins (HSP 70) in HeLa tumor cells treated with increasing concentrations of the AuNR/GO nanohybrid as mentioned, monitored by flow cytometry either in dark conditions or under NIR (808 nm) laser treatment (300 mW) for 5 min. (E) Calcein AM/PI costained cellular images of HeLa cells after indicated treatments.

up to 58.4 °C, which is possibly because of the synergistic plasmonic photothermal effect (Figure 3B). Compared to the AuNR/GO hybrid, the mixture of AuNRs and GO aqueous suspension shows a ΔT (19.4 °C), which is almost half of the AuNR/GO hybrid. Thus, the better PTT performance of the AuNR/GO hybrid than either their mixture or a single agent verifies that the high PTT efficiency is possibly because of the synergistic PPTT effect induced by the plasmonic nanohybrid (Figure S6A,B). The digital photographs showing the real-time temperature increase by different groups are also displayed in Figure 3C. Additionally, the plasmonic nanohybrid exhibits concentration-dependent PTT performance, as a significant temperature increase from 26.1 to 56.4 °C is observed with an increase in the concentration from 10 to 100 μg/mL (Figure S7A). As a control, no noticeable temperature increase was observed in the case of PBS under similar conditions. Power-dependent PTT performance is also noticed as a maximum temperature increase up to 90.7 °C occurs for the AuNR@GO hybrid under high laser power irradiation (750 mW) as shown in Figure S7B.

Keeping in mind the risks of skin burns and damage to normal tissues caused by the use of high-power laser and making the designed plasmonic nanohybrid more translational from proof of concept to practical clinical applications, we chose 300 mW laser power density for antibacterial and anticancer PTT *in vitro*. It is noteworthy to mention that the chosen laser power density is still below the guidelines of the American National Standard Institute (ANSI). Meanwhile, no noticeable decrease has been observed in the PTT performance of AuNRs/GO using this low laser power density after four different laser on/off cycles (Figure 3D). Furthermore, the SEM imaging of AuNRs/GO after four cycles of laser irradiation does not show any particular change in the structure of AuNRs, indicating the appreciable PTT stability of the AuNR@GO nanohybrid for PTT therapy (Figure S8). Importantly, photothermal conversion efficiency (PCE) calculations indicate a far superior PCE (72.59%) of the

DOI: 10.1021/acsabm.9b00521
ACS Appl. Bio Mater. 2019, 2, 3942−3953

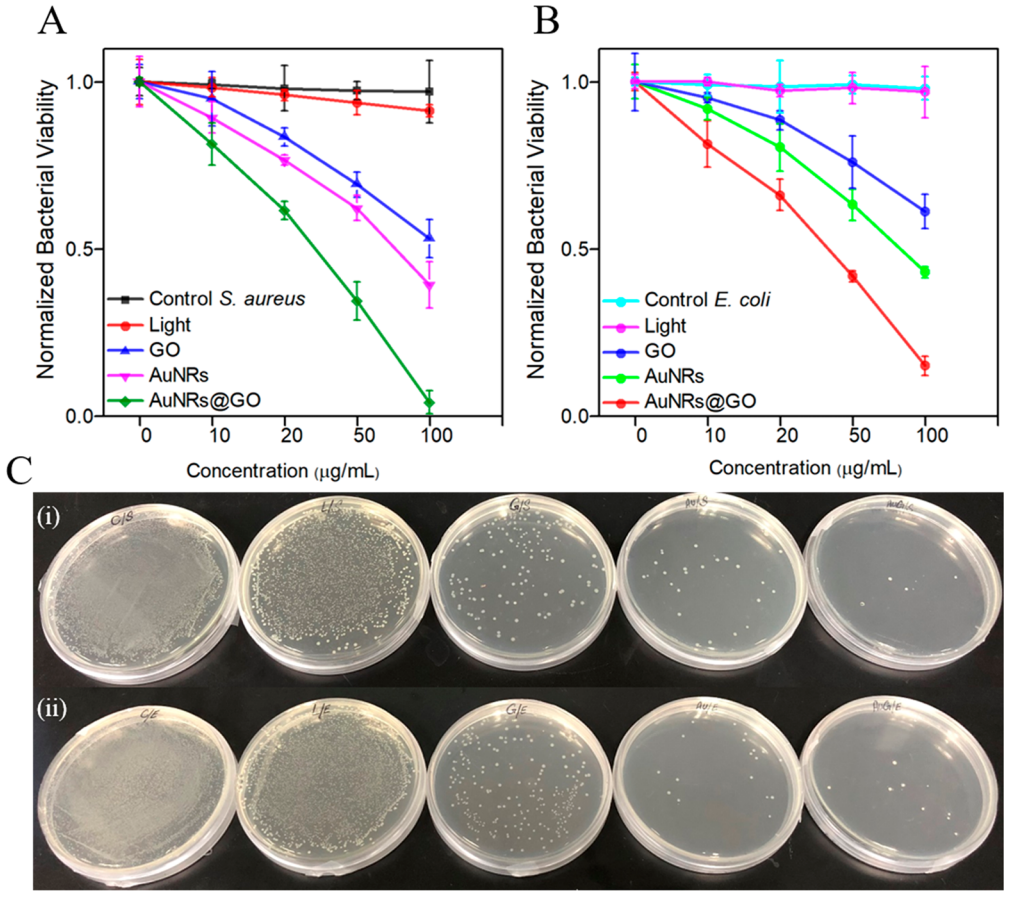

Figure 6. Antibacterial PTT. Normalized bacterial viability of *S. aureus* (A) and *E. coli* (B) treated with different concentrations of indicated materials following 808 nm laser excitation (300 mW) for 5 min. (C) Digital micrographs of the plates showing the viable colonies of *S. aureus* (i) and *E. coli* (ii) under different conditions. Left to right shows the control experiments: no light, only light, GO nanosheets, AuNRs, and the AuNR@GO nanohybrid, following 808 nm laser treatment (300 mW) for 5 min.

AuNR/GO nanohybrid than either individual GO nanosheets (18%) or AuNRs (35%), which strongly proves the existence of a synergistic plasmonic effect by the dual plasmonic photothermal nanoagents (PPTAs) (Figure 4A–F). A summary and comparison of the previously developed PTAs with the present work have been shown in Table S1. The high PCE by the plasmonic nanohybrid is strongly ascribed to the synergistic PPTT effect, enhanced localized electromagnetic field, and low scattering loss.

Before investigating the PTT applications, we investigated the cellular uptake capacity of AuNRs/GO in HeLa cells by monitoring the *in vitro* fluorescence of FITC. Interestingly, the fluorescence intensity gradually increases with the uptake time and reaches the maximum value at 24 h (Figure 5A). It is also noticed that a higher concentration of the AuNR/GO nanohybrid (100 μg/mL) demonstrates an enhanced cellular uptake as compared to the lower concentration (10 μg/mL) as evidenced by the change in fluorescence intensity of FITC (Figure S9). These findings suggest that the plasmonic nanohybrid can be efficiently uptaken by the cells and thus is capable of inducing localized photothermal killing of cancerous cells/bacterial pathogens under laser activation. Thus, effective cellular uptake and excellent PTT stability encourage us to quantitatively determine the anticancer phototherapeutic applications of the AuNR/GO nanohybrid. However, as the stability of the therapeutic agent in biological media is an important factor which determines the overall therapeutic efficacy, we studied the stability of AuNRs/GO in PBS, DI H_2O, ethanol, and culture medium (DMEM with 10% FBS). No noticeable aggregation is observed as shown by the digital micrographs in Figure S10A, indicating the excellent colloidal solubility of AuNRs/GO in the given media. Moreover, the UV–vis absorption spectra of the plasmonic AuNR/GO hybrid do not show any change either prior to or after (2, 6, 12, 24, 48, and 72 h) postincubation in biological media such as PBS with 10% FBS (Figure S10B). Hence, these results strongly suggest the efficient stability of AuNRs/GO in biological media. Therefore, we next determined the biocompatibility and dark cytotoxicity of the AuNR/GO nanohybrid *in vitro* against normal human cell line (HUVECs) and HeLa tumor cells by a standard MTT assay. It has been noted that the AuNRs/GO do not reduce the cellular viability in dark conditions, suggesting the noncytotoxicity and biocompatibility of the designed plasmonic hybrid (Figure 5B). However, under light activation (808 nm, 0.3 W/cm^2), AuNRs/GO demonstrate dose-dependent phototherapeutic behavior as the cellular viability is substantially decreased from 97.24% to 4.17% at a higher dose of 0.1 mg/mL. The higher cellular destruction is strongly ascribed to the synergistic PPTT effect of dual plasmonic photothermal nanoagents (PTAs). The photothermal killing efficiency of the plasmonic nanohybrid is also significantly higher than the individual PTA-like GO nanosheets (34.92%) and AuNRs (19.24%), respectively, which further confirm the existence of synergistic

DOI: 10.1021/acsabm.9b00521
ACS Appl. Bio Mater. 2019, 2, 3942–3953

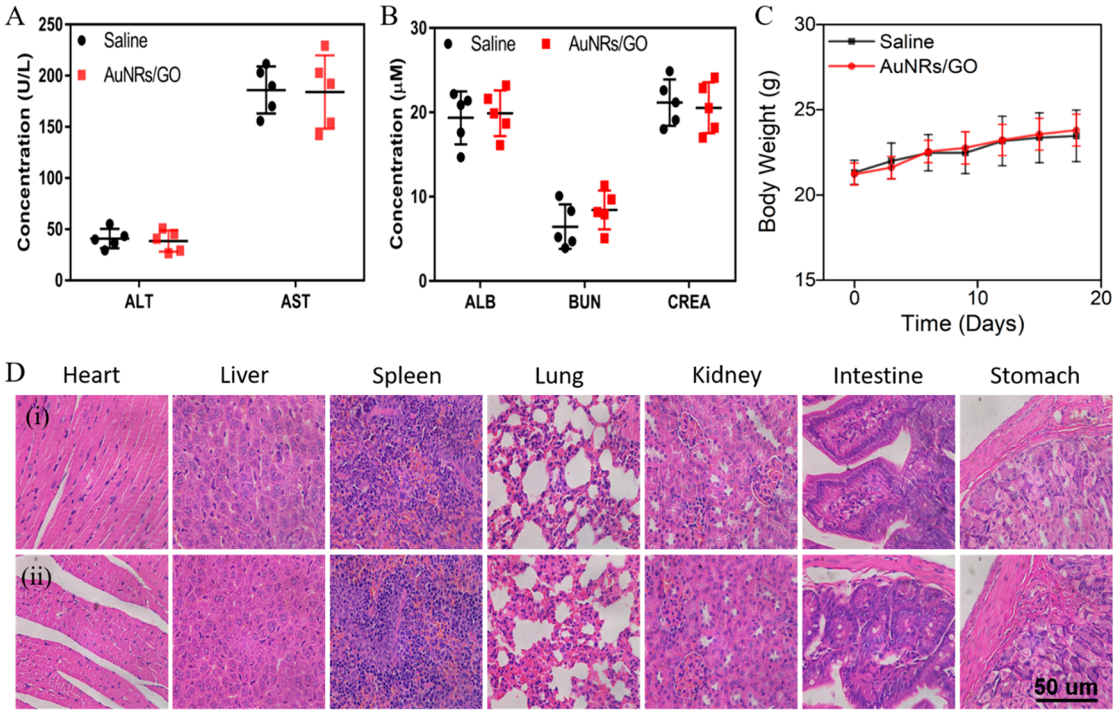

Figure 7. *In vivo* biocompatibility evaluation. (A–C) Blood biochemical analysis as well as body weight of the control and experimental group after treatment with saline or the intravenously (i.v.) injected AuNR/GO hybrid (100 μg/mL, 100 μL) for about 18 days. Body weight was recorded after every 2 days. H&E staining analysis of the major organs as mentioned, collected from both the groups after 18 days treated with either saline (i) or (ii) the AuNR/GO hybrid, respectively (D).

plasmonic photothermal therapy (Figure 5C). To confirm that the higher cellular destruction is solely due to the synergistic PPTT, we examined the expression of heat shock proteins (HSP 70) in HeLa tumor cells treated with the AuNR/GO nanohybrid followed by 808 nm laser excitation (300 mW) for 5 min.

HSP 70 proteins are the molecular chaperones which will be overexpressed in response to the heat stress and thus can serve as a sensitive indicator of the extreme heat stress. Generally, when the inner temperature of a cell crosses a threshold value (42 °C) for a short time, HSP 70 induces protein refolding and simultaneously inhibits the apoptotic pathway via cytochrome C and caspase pathways, leading to an enhanced thermotolerance of cells. Impressively, compared to the control groups, the percentage of HeLa tumor cells overexpressing HSP 70 is significantly higher (about 6-fold), which verifies that the tumor cells killing is entirely due to the enhanced PCE and localized hyperthermia generated by the plasmonic AuNR/GO nanohybrid under low power laser activation (Figure 5D). Live/Dead assay was further performed to investigate the *in vitro* phototherapeutic performance using Calcein AM/PI cellular staining. Under dark conditions, no cellular deaths are observed as most of the cells exhibit green fluorescence. However, a partial cellular destruction is noticed in the case of either GO or AuNRs after laser treatment, respectively, whereas because of the synergistic PPTT effect, AuNRs/GO induce complete cellular destruction as indicated by the red fluorescence of PI (Figure 5E). Furthermore, the plasmonic AuNR/GO hybrid also demonstrates concentration-dependent cellular killing, as the ratio of the dead cells increases with increasing the concentration of the hybrid material to 100 μg/mL, and all the cells exhibit red fluorescence, confirming their nonviability (Figure S11).

After the successful demonstration of an impressive synergistic anticancer PPTT, we further extend our investigations to explore the antibacterial PPTT performance of the AuNR/GO nanohybrid against both *S. aureus* and *E. coli*. Keeping in mind that the bacterial pathogens are usually resistant to antibiotics, localized photothermal killing is an ideal approach to eradicate antibiotic-resistant pathogens. Both the *S. aureus* and *E. coli*, respectively, were incubated with varying concentrations of the plasmonic AuNR/GO nanohybrid, following NIR laser treatment for 5 min. The viability of both the *S. aureus* and *E. coli* is remarkably reduced to 4.049% and 14.94%, respectively, at a higher dose of 100 μg/mL of the AuNR/GO nanohybrid (Figure 6A,B).

The digital photographs of the plates showing the viable bacterial colonies are also presented in Figure 6C. It is found that the Gram-negative *E. coli* bacteria possesses a thick peptidoglycan layer which makes them less susceptible to photothermal killing. However, antibacterial PTT efficacy of the plasmonic AuNR/GO nanohybrid against both the Gram +ve as well as the Gram −ve bacteria is significantly higher than the individual PTAs such as GO nanosheets and AuNRs, respectively, implying the enhanced synergistic phototherapeutic performance. Meanwhile, no obvious decrease in bacterial viability is observed in either dark conditions or only under laser irradiation, suggesting that laser light alone is not capable of killing the bacterial pathogens.

To ensure the practical phototherapeutic applications of the AuNR/GO hybrid, *in vivo* biocompatibility investigations were performed on healthy nude mice for about 18 days. Impressively, the body weight of both the control and experimental groups did not show any change. Similarly, blood biochemical analysis also suggests that both the kidney and liver work normally as no significant changes are noticed in

DOI: 10.1021/acsabm.9b00521
ACS Appl. Bio Mater. 2019, 2, 3942–3953

the levels of creatinine (CREA), blood urea nitrogen (BUN), albumin (ALB), aspartate aminotransferase (AST), and alkaline phosphatase (ALP), as shown in Figure 7A–C. These results are in strong accordance with the reported literature.[42] Moreover, H&E staining analysis of the major organs (stomach, liver, intestine, kidney, lung, spleen, and heart) collected from the mice treated with the AuNR/GO hybrid does not reveal any particular histopathological change, suggesting the excellent *in vivo* biocompatibility and nontoxicity (Figure 7D). Hence, following our concept, different hybrid-based PTAs could be developed to achieve high PCE under low power laser excitation and thus make them equally applicable for both antibacterial as well as anticancer therapy, respectively. In addition, *in vitro* therapeutic performance and the *in vivo* biocompatibility strongly advocate the practical feasibility and safety of plasmonic hybrid-based PTAs for *in vivo* translation.

CONCLUSIONS

In summary, we have successfully designed a highly efficient plasmonic phototherapeutic nanohybrid capable of inducing enhanced photothermal ablation of bacterial pathogens/tumor cells. We demonstrate that by combining dual plasmonic photothermal nanoagents high PCE could be achieved due to the synergistic plasmonic PTT effects. Importantly, the plasmonic AuNR/GO hybrid exhibits significantly higher PCE than previously reported photothermal nanoagents under low laser power density, facilitating the remarkable antibacterial/anticancer PTT within a short treatment time. The synergistic antibacterial/anticancer PPTT effects induced by the plasmonic nanohybrid are far superior to the individual PTAs of either GO or AuNRs, respectively. In a nutshell, owing to the high PCE under low laser power excitation, the plasmonic nanohybrid will surely emerge as a benchmark photothermal agent, offering high therapeutic index with reduced skin phototoxicity, leading to a shift in the cancer PTT from bench to bedside.

ASSOCIATED CONTENT

Supporting Information

The Supporting Information is available free of charge on the ACS Publications website at DOI: 10.1021/acsabm.9b00521.

AFM and FTIR analysis of GO nanosheets; SEM, EDX elemental mapping, and DLS analysis of AuNRs, GO, and the AuNR/GO nanohybrid; photothermal performance; cellular uptake; and comparison of the reported literature (Table S1) (PDF)

AUTHOR INFORMATION

Corresponding Author

*E-mail: xhxia@nju.edu.cn.

ORCID

Shouju Wang: 0000-0001-9213-6818
Deju Ye: 0000-0002-9887-0914
Xing-Hua Xia: 0000-0001-9831-4048

Notes

The authors declare no competing financial interest.

ACKNOWLEDGMENTS

This work was supported by the grants from the National Key R&D Program of China (2017YFA0700500) and the National Natural Science Foundation of China (21635004).

REFERENCES

(1) Lee, D.-E.; Koo, H.; Sun, I.-C.; Ryu, J. H.; Kim, K.; Kwon, I. C. Multifunctional Nanoparticles for Multimodal Imaging and Theragnosis. *Chem. Soc. Rev.* **2012**, *41*, 2656–2672.

(2) Woodford, N.; Livermore, D. M. Infections Caused by Gram-Positive Bacteria: A Review of the Global Challenge. *J. Infect.* **2009**, *59*, 4–16.

(3) Satpathy, S.; Sen, S. K.; Pattanaik, S.; Raut, S. Review on Bacterial Biofilm: An Universal Cause of Contamination. *Biocatal. Agric. Biotechnol.* **2016**, *7*, 56–66.

(4) Chabner, B. A.; Roberts, T. G., Jr Chemotherapy and the War on Cancer. *Nat. Rev. Cancer* **2005**, *5*, 65.

(5) Tamura, R. E.; Lana, M. G.; Costanzi-Strauss, E.; Strauss, B. E. Combination of Cabazitaxel and p53 Gene Therapy Abolishes Prostate Carcinoma Tumor Growth. *Gene Ther.* **2019**, DOI: 10.1038/s41434-019-0071-x.

(6) Atkins, S.; He, F. Chemotherapy and Beyond: Infections in the Era of Old and New Treatments for Hematologic Malignancies. *Infectious Disease Clinics of North America* **2019**, *33*, 289–309.

(7) Geller, L. T.; Barzily-Rokni, M.; Danino, T.; Jonas, O. H.; Shental, N.; Nejman, D.; Gavert, N.; Zwang, Y.; Cooper, Z. A.; Shee, K.; Thaiss, C. A.; Reuben, A.; Livny, J.; Avraham, R.; Frederick, D. T.; Ligorio, M.; Chatman, K.; Johnston, S. E.; Mosher, C. M.; Brandis, A.; Fuks, G.; Gurbatri, C.; Gopalakrishnan, V.; Kim, M.; Hurd, M. W.; Katz, M.; Fleming, J.; Maitra, A.; Smith, D. A.; Skalak, M.; Bu, J.; Michaud, M.; Trauger, S. A.; Barshack, I.; Golan, T.; Sandbank, J.; Flaherty, K. T.; Mandinova, A.; Garrett, W. S.; Thayer, S. P.; Ferrone, C. R.; Huttenhower, C.; Bhatia, S. N.; Gevers, D.; Wargo, J. A.; Golub, T. R.; Straussman, R. Potential Role of Intratumor Bacteria in Mediating Tumor Resistance to the Chemotherapeutic Drug Gemcitabine. *Science* **2017**, *357*, 1156–1160.

(8) Sougiannis, A. T.; VanderVeen, B. N.; Enos, R. T.; Velazquez, K. T.; Bader, J. E.; Carson, M.; Chatzistamou, I.; Walla, M.; Pena, M. M.; Kubinak, J. L.; Nagarkatti, M.; Carson, J. A.; Murphy, E. A. Impact of 5 Fluorouracil Chemotherapy on Gut Inflammation, Functional Parameters, and Gut Microbiota. *Brain, Behav., Immun.* **2019**, *80*, 44.

(9) Lucky, S. S.; Soo, K. C.; Zhang, Y. Nanoparticles in Photodynamic Therapy. *Chem. Rev.* **2015**, *115*, 1990–2042.

(10) Castano, A. P.; Mroz, P.; Hamblin, M. R. Photodynamic Therapy and Anti-Tumour Immunity. *Nat. Rev. Cancer* **2006**, *6*, 535–45.

(11) Zheng, D. W.; Li, B.; Li, C. X.; Fan, J. X.; Lei, Q.; Li, C.; Xu, Z.; Zhang, X. Z. Carbon-Dot-Decorated Carbon Nitride Nanoparticles for Enhanced Photodynamic Therapy against Hypoxic Tumor *via* Water Splitting. *ACS Nano* **2016**, *10*, 8715–22.

(12) Yang, G.; Xu, L.; Chao, Y.; Xu, J.; Sun, X.; Wu, Y.; Peng, R.; Liu, Z. Hollow MnO_2 as a Tumor-Microenvironment-Responsive Biodegradable Nano-platform for Combination Therapy Favoring Antitumor Immune Responses. *Nat. Commun.* **2017**, *8*, 902.

(13) Jung, H. S.; Verwilst, P.; Sharma, A.; Shin, J.; Sessler, J. L.; Kim, J. S. Organic Molecule-Based Photothermal Agents: An Expanding Photothermal Therapy Universe. *Chem. Soc. Rev.* **2018**, *47*, 2280–2297.

(14) Liu, Y.; Bhattarai, P.; Dai, Z.; Chen, X. Photothermal Therapy and Photoacoustic Imaging *via* Nanotheranostics in Fighting Cancer. *Chem. Soc. Rev.* **2019**, *48*, 2053–2108.

(15) Pu, K. A Smart Supramolecular Phototherapeutics for Specific Cancer Therapy. *Sci. China: Chem.* **2018**, *61*, 1353–1354.

(16) Cheng, L.; Wang, C.; Feng, L.; Yang, K.; Liu, Z. Functional Nanomaterials for Phototherapies of Cancer. *Chem. Rev.* **2014**, *114*, 10869–10939.

DOI: 10.1021/acsabm.9b00521
ACS Appl. Bio Mater. 2019, 2, 3942–3953

(17) Abbas, M.; Zou, Q.; Li, S.; Yan, X. Self-Assembled Peptide- and Protein-Based Nanomaterials for Antitumor Photodynamic and Photothermal Therapy. *Adv. Mater.* **2017**, *29*, 1605021.
(18) Li, J.; Xie, C.; Huang, J.; Jiang, Y.; Miao, Q.; Pu, K. Semiconducting Polymer Nanoenzymes with Photothermic Activity for Enhanced Cancer Therapy. *Angew. Chem., Int. Ed.* **2018**, *57*, 3995−3998.
(19) Mateo, D.; Esteve-Adell, I.; Albero, J.; Royo, J. F.; Primo, A.; Garcia, H. 111 Oriented Gold Nanoplatelets on Multilayer Graphene as Visible Light Photocatalyst for Overall Water Splitting. *Nat. Commun.* **2016**, *7*, 11819.
(20) Shi, Y.; Zhang, Q.; Zhai, T.-T.; Zhou, Y.; Yang, D.-R.; Wang, F.-B.; Xia, X.-H. Localized Surface Plasmon Resonance Enhanced Label-Free Photoelectrochemical Immunoassay by Au-MoS_2 Nanohybrid. *Electrochim. Acta* **2018**, *271*, 361−369.
(21) Li, X.; Zhu, J.; Wei, B. Hybrid Nanostructures of Metal/Two-Dimensional Nanomaterials for Plasmon-Enhanced Applications. *Chem. Soc. Rev.* **2016**, *45*, 3145−87.
(22) Hong, J. W.; Wi, D. H.; Lee, S. U.; Han, S. W. Metal-Semiconductor Heteronanocrystals with Desired Configurations for Plasmonic Photocatalysis. *J. Am. Chem. Soc.* **2016**, *138*, 15766−15773.
(23) Shen, S.; Zhu, C.; Huo, D.; Yang, M.; Xue, J.; Xia, Y. A Hybrid Nanomaterial for the Controlled Generation of Free Radicals and Oxidative Destruction of Hypoxic Cancer Cells. *Angew. Chem., Int. Ed.* **2017**, *56*, 8801−8804.
(24) Waiskopf, N.; Ben-Shahar, Y.; Galchenko, M.; Carmel, I.; Moshitzky, G.; Soreq, H.; Banin, U. Photocatalytic Reactive Oxygen Species Formation by Semiconductor-Metal Hybrid Nanoparticles. Toward Light-Induced Modulation of Biological Processes. *Nano Lett.* **2016**, *16*, 4266−4273.
(25) Cheng, K.; Sano, M.; Jenkins, C. H.; Zhang, G.; Vernekohl, D.; Zhao, W.; Wei, C.; Zhang, Y.; Zhang, Z.; Liu, Y.; Cheng, Z.; Xing, L. Synergistically Enhancing the Therapeutic Effect of Radiation Therapy with Radiation Activatable and Reactive Oxygen Species-Releasing Nanostructures. *ACS Nano* **2018**, *12*, 4946−4958.
(26) Banin, U.; Ben-Shahar, Y.; Vinokurov, K. Hybrid Semiconductor−Metal Nanoparticles: From Architecture to Function. *Chem. Mater.* **2014**, *26*, 97−110.
(27) Du, Y.; Jiang, Q.; Beziere, N.; Song, L.; Zhang, Q.; Peng, D.; Chi, C.; Yang, X.; Guo, H.; Diot, G.; Ntziachristos, V.; Ding, B.; Tian, J. DNA-Nanostructure-Gold-Nanorod Hybrids for Enhanced *In Vivo* Optoacoustic Imaging and Photothermal Therapy. *Adv. Mater.* **2016**, *28*, 10000−10007.
(28) Aioub, M.; Panikkanvalappil, S. R.; El-Sayed, M. A. Platinum-Coated Gold Nanorods: Efficient Reactive Oxygen Scavengers That Prevent Oxidative Damage toward Healthy, Untreated Cells during Plasmonic Photothermal Therapy. *ACS Nano* **2017**, *11*, 579−586.
(29) Zhu, H.; Wang, Y.; Chen, C.; Ma, M.; Zeng, J.; Li, S.; Xia, Y.; Gao, M. Monodisperse Dual Plasmonic Au@Cu_2-xE (E= S, Se) Core@Shell Supraparticles: Aqueous Fabrication, Multimodal Imaging, and Tumor Therapy at *in Vivo* Level. *ACS Nano* **2017**, *11*, 8273−8281.
(30) Leng, C.; Zhang, X.; Xu, F.; Yuan, Y.; Pei, H.; Sun, Z.; Li, L.; Bao, Z. Engineering Gold Nanorod-Copper Sulfide Heterostructures with Enhanced Photothermal Conversion Efficiency and Photostability. *Small* **2018**, *14*, 1703077.
(31) Younis, M. R.; Wang, C.; An, R.; Wang, S.; Younis, M. A.; Li, Z. Q.; Wang, Y.; Ihsan, A.; Ye, D.; Xia, X. H. Low Power Single Laser Activated Synergistic Cancer Phototherapy Using Photosensitizer Functionalized Dual Plasmonic Photothermal Nanoagents. *ACS Nano* **2019**, *13*, 2544−2557.
(32) Shi, Y.; Wang, J.; Wang, C.; Zhai, T. T.; Bao, W. J.; Xu, J. J.; Xia, X. H.; Chen, H. Y. Hot Electron of Au Nanorods Activates the Electrocatalysis of Hydrogen Evolution on MoS_2 Nanosheets. *J. Am. Chem. Soc.* **2015**, *137*, 7365−7370.
(33) Tan, C.; Cao, X.; Wu, X. J.; He, Q.; Yang, J.; Zhang, X.; Chen, J.; Zhao, W.; Han, S.; Nam, G. H.; Sindoro, M.; Zhang, H. Recent Advances in Ultrathin Two-Dimensional Nanomaterials. *Chem. Rev.* **2017**, *117*, 6225−6331.
(34) Jin, H.; Guo, C.; Liu, X.; Liu, J.; Vasileff, A.; Jiao, Y.; Zheng, Y.; Qiao, S. Z. Emerging Two-Dimensional Nanomaterials for Electrocatalysis. *Chem. Rev.* **2018**, *118*, 6337−6408.
(35) Yin, P. T.; Shah, S.; Chhowalla, M.; Lee, K.-B. Design, Synthesis, and Characterization of Graphene−Nanoparticle Hybrid Materials for Bioapplications. *Chem. Rev.* **2015**, *115*, 2483−2531.
(36) Chen, Y. W.; Su, Y. L.; Hu, S. H.; Chen, S. Y. Functionalized Graphene Nanocomposites for Enhancing Photothermal Therapy in Tumor Treatment. *Adv. Drug Delivery Rev.* **2016**, *105*, 190−204.
(37) Wu, C.; Zhu, A.; Li, D.; Wang, L.; Yang, H.; Zeng, H.; Liu, Y. Photosensitizer-Assembled PEGylated Graphene-Copper Sulfide Nanohybrids as a Synergistic Near-Infrared Phototherapeutic Agent. *Expert Opin. Drug Delivery* **2016**, *13*, 155−165.
(38) Bai, J.; Liu, Y.; Jiang, X. Multifunctional PEG-GO/CuS Nanocomposites for Near-Infrared Chemo-Photothermal Therapy. *Biomaterials* **2014**, *35*, 5805−5813.
(39) Wu, C.; Li, D.; Wang, L.; Guan, X.; Tian, Y.; Yang, H.; Li, S.; Liu, Y. Single Wavelength Light-Mediated, Synergistic Bimodal Cancer Photoablation and Amplified Photothermal Performance by Graphene/Gold Nanostar/Photosensitizer Theranostics. *Acta Biomater.* **2017**, *53*, 631−642.
(40) Wang, J.; Wang, K.; Wang, F.-B.; Xia, X.-H. Bioinspired Copper Catalyst Effective for both Reduction and Evolution of Oxygen. *Nat. Commun.* **2014**, *5*, 5285.
(41) Ye, X.; Zheng, C.; Chen, J.; Gao, Y.; Murray, C. B. Using Binary Surfactant Mixtures to Simultaneously Improve the Dimensional Tunability and Monodispersity in the Seeded Growth of Gold Nanorods. *Nano Lett.* **2013**, *13*, 765−771.
(42) Wang, S.; Ma, X.; Hong, X.; Cheng, Y.; Tian, Y.; Zhao, S.; Liu, W.; Tang, Y.; Zhao, R.; Song, L.; Teng, Z.; Lu, G. Adjuvant Photothermal Therapy Inhibits Local Recurrences after Breast-Conserving Surgery with Little Skin Damage. *ACS Nano* **2018**, *12*, 662−670.

DOI: 10.1021/acsabm.9b00521
ACS Appl. Bio Mater. 2019, 2, 3942−3953